International Journal of Mechanical and Electrical Engineering

ISSN: 3005-9615 (Print), ISSN: 3005-7132 (Online) | Volume 5, Number 3, Year 2025
DOI: https://doi.org/10.62051/ijmee.v5n3.02
Journal homepage: https://wepub.org/index.php/IJMEE/index

Mechanical Analysis and Structural Optimization of Anchorage for Split Segment Inserted Tooth Slips

Kaixin Lv *, Zhongzhi Hu [a]

College of Mechanical Engineering, Sichuan University of Science & Engineering, Yibin, Sichuan, 643002, China

* Corresponding author: Kaixin Lv (Email: 2252543198@qq.com), [a] zhongzhi-hu@suse.edu.cn

ABSTRACT

This study investigates the anchoring capacity issues pertaining to internally-fitted inserted tooth slips within 140-grade casing pipes. By conducting static analysis, a formula linking tooth stress to tooth diameter, tooth inclination angles (both frontal and rear), and the base inclination angle has been formulated. Utilizing orthogonal testing and finite element simulations, the structural parameters of segmented toothed slips were refined. The findings reveal that by setting the tooth diameter at 7mm, the base wedge angle at 18°, the tooth groove angle at 55°, the tooth height at 6.5mm, and the circumferential angle at 8°, there is a notable enhancement in the evenness of stress distribution between the teeth and casing, resulting in a more balanced anchoring effect.

KEYWORDS

Toothed Slips Orthogonal Testing; Finite Element Static Analysis.

1. INTRODUCTION

As the continuous exploitation of formations progresses, China's shallow-to-medium oil and gas resources are dwindling, rendering the exploitation of deep and ultra-deep wells a crucial avenue for securing future hydrocarbon resources [1-3]. In recent years, China has witnessed a steady increase in the number and depths of ultra-deep and extremely deep wells, with ultra-deep wells exceeding 8,000 meters becoming the norm, and drilling projects for wells reaching 10,000 meters are underway. Taking the Deep Earth TK1 and CK1 wells drilled by China National Petroleum Corporation in the Tarim and Sichuan basins in 2023 as examples, their designed vertical depths have reached 11,100 meters and 10,520 meters, respectively [4-6]. Due to the escalating complexity of geological conditions with increasing well depths, China has developed the TP140V oil casing to cater to the needs of ultra-deep well development [7-9].The slip packer, which achieves sealing and anchoring through the contact between rubber sleeves, slips, and casing, encounters challenges in deep and ultra-deep wells where the use of ultra-high steel-grade casing can lead to shallow slip tooth penetration into the casing, resulting in unstable anchoring and subsequent seal failure [10-13].As a crucial component of the packer, the selection of slip material and design of its structure significantly impact anchoring reliability. To meet the demand for high anchoring performance within higher steel-grade casing, slips must be fabricated from materials with greater strength.

Two types of slip structures can be chosen: milled-tooth slips and insert-tooth slips [14]. Milled-tooth slips feature multiple rows of teeth on their surface, processed through milling, whereas insert-tooth slips involve separate processing of the slip base and tooth inserts. When opting for high-strength slip materials, the use of carbide inserts and a lower-strength slip base results in lower processing costs compared to the monolithic processing of milled-tooth slips. Furthermore, the structure of insert-tooth slips significantly reduces the overall length of the setting tool, enhancing safety during operations [15].

Recently, scholars have conducted research on various structural designs of insert-tooth slips. Zhang Derong [16] et al. investigated the impact of primary structural parameters of tooth inserts and milled teeth on anchoring performance. Yu Bing [17] et al. summarized the influence of changes in tooth groove axis angle during anchoring on contact pressure on the casing inner wall. Wang Zhijian [18] et al. studied the influence of tooth spacing on the safety of slip setting. Feng Wenrong [19] et al. analyzed the reliability of slip setting by examining the furrow shapes formed after contact between different types of insert-tooth slips and casing, as well as the displacement and stress between the casing and tooth inserts. Lu Jiankang [20] et al. established a force balance relationship between the slip and cone by analyzing the force conditions during slip anchoring and studied the influence of variations in slip tooth installation hole diameter and slip bevel cone angle on stress at the bottom of insert installation holes. Their findings indicate that adjusting the hole diameter and slip bevel cone angle can alleviate stress concentration at the bottom of insert installation holes.

The aforementioned studies focused on optimizing and evaluating slip structural parameters for anchoring with steel-grade casing such as P110. However, their applicability to casing with higher strength grades remains to be assessed. Consequently, this paper takes the slips of the RTTS packer as the research object. Through finite element numerical simulation and orthogonal experimental analysis, we analyze the stress-strain patterns of the slip base and tooth inserts during the anchoring process of insert-tooth slips with TP140V casing, thereby optimizing the geometric parameters of the slips. The research findings provide valuable reference for the structural design and optimization of packer slips within casing with higher steel grades.

2. MECHANICAL ANALYSIS OF THE INSERTED TOOTH SLIP

During the operation of the packer slip, the cone moves axially under the action of the setting load. When the wedge surface of the cone contacts the inclined surface of the slip base, the slip moves radially, so that the slip inserts are in contact with the casing. By increasing the setting load, the inserts gradually bite into the inner wall of the casing to realize the packer positioning[21].

The anchoring mechanism is simplified into components consisting of cone, slip base, slip insert teeth and casing, and its force analysis is shown in Fig.1.

The upper end face of the cone is subject to axial force F, the wedge-shaped surface of the slip base is subject to normal and tangential component forces R and f, and the horizontal and vertical component forces N and F_t of the insert teeth are acted on by the sleeve. According to the principle of static equilibrium, the force analysis of slips is obtained:

$$F = R\sin\beta + f\cos\beta \tag{1}$$

Where: F is the axial force on the cone, R is the normal component force on the single slip, f is the tangential component force on the single slip, and β is the cone Angle of the slip base.

The relationship between the tangential component force f acting on the wedge face of the slip base and the friction coefficient is:

$$f = \mu R \tag{2}$$

Where: μ is the friction coefficient between the slip and the casing.

$$\mu = \tan\varphi \tag{3}$$

Where: φ is the friction Angle between the slip and the cone, °.

$$N = R\cos\beta - f\sin\beta \tag{4}$$

Where: N is the horizontal component force on a single slip, N.

From formula (1) to formula (4), it can be obtained that the horizontal component N of a single slip is

$$N = \frac{F}{\tan(\beta + \varphi)} \tag{5}$$

Fig.2 is a diagram of insert insert casing. The following geometric relationship can be obtained from the figure:

$$h = \frac{b}{\tan\alpha_1 + \tan\alpha_2} \tag{6}$$

Where: h is the depth at which the casing is embedded, mm, b is the contact length between the tooth and the casing, mm, α_1 is the front inclination of the tooth, °, α_2 is the back inclination of the tooth, °.

The contact area S between the tooth and the casing is calculated approximately after the inserted tooth are inserted into the casing:

$$S = \frac{\pi d b \phi}{360°} \tag{7}$$

Where: ϕ is the contact Angle between the insert circle and the casing, °, and d is the diameter of the upper round surface of the inserted tooth, mm.

The contact stress σ between the inserted tooth and casing can be obtained by connecting the formula (5) to formula (7):

$$\sigma = \frac{N}{S} = \frac{360°F}{\pi d h \phi \tan(\beta + \varphi)(\tan\alpha_1 + \tan\alpha_2)} \tag{8}$$

Where: σ is the contact stress between the inserted tooth and casing, MPa.

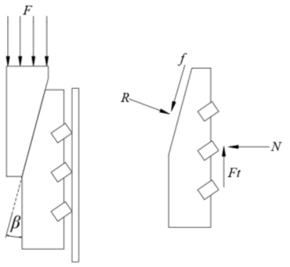

Fig 1. Slip force analysis diagram

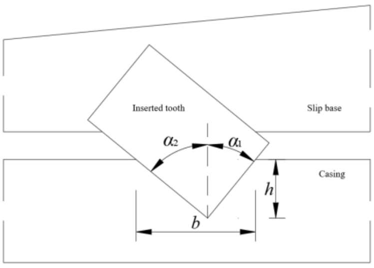

Fig 2. Inserted tooth inserts casing diagram

3. FINITE ELEMENT ANALYSIS OF ANCHORING MECHANISM

3.1. Finite Element Simulation Model

The tooth-embedded slip anchoring mechanism comprises six symmetrically arranged slip bases. To enhance numerical simulation efficiency while ensuring computational accuracy, one-sixth of the entire mechanism is analyzed for anchoring performance, as depicted in Figure 3. The three-dimensional model features a casing diameter of 177.8mm and a wall thickness of 12.65mm. The teeth are numbered from 1 to 6, with the upper cylindrical edge chamfered at a curvature radius of 0.2mm [22]. Figure 4 illustrates the tooth-embedded slip structure, with tooth height h set at 6mm, tooth diameter d at 5mm, a circumferential angle θ of 10°, a substrate wedge angle γ of 12°, and a tooth groove inclination angle α of 60°.

3.2. Material Parameter

TP140V steel is selected as the casing material, with its stress-strain curve presented in Figure 5. High-strength alloy steel 20Cr2Ni4 is utilized for the cone and slip base materials [23], while ZD10U carbide material is chosen for the teeth. The specific material parameters are listed in Table 1.

3.3. Mesh Generation

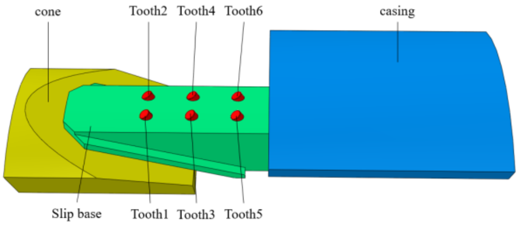

Fig 3. Assembly model of single slip

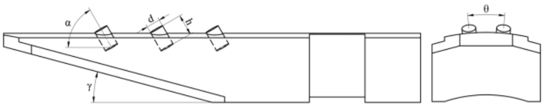

Fig 4. Diagram of slip structure parameters

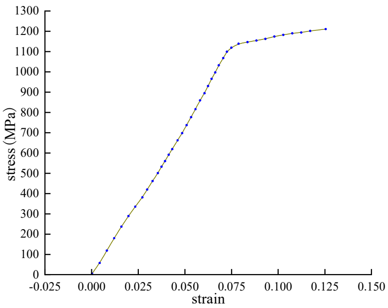

Fig 5. Stress-strain curve of TP140V

A finite element model of the tooth-embedded slip is established and meshed as shown in Figure 6. Given that the tooth-casing and tooth-slip base contact regions are the primary analysis targets, mesh refinement levels in these areas are varied during mesh independence verification, with results presented in Figure 7. Mesh independence analysis indicates that when mesh size is reduced below 0.6mm, the sensitivity of computational results to mesh density gradually diminishes. Specifically, the penetration depth increases from 0.3588mm to 0.3687mm, with a variation of less than 3%, while casing contact stress increases from 1187MPa to 1189MPa, a change of under 1%. Thus, balancing computational efficiency and accuracy, a 0.4mm mesh is selected for subsequent simulations.

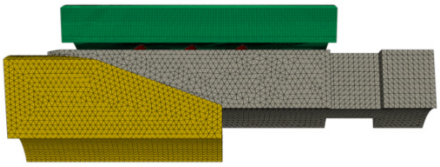

a.global meshing

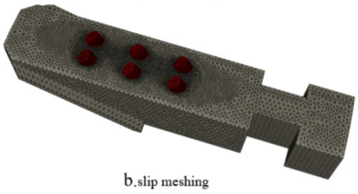

b.slip meshing

Fig 6. Grid diagram

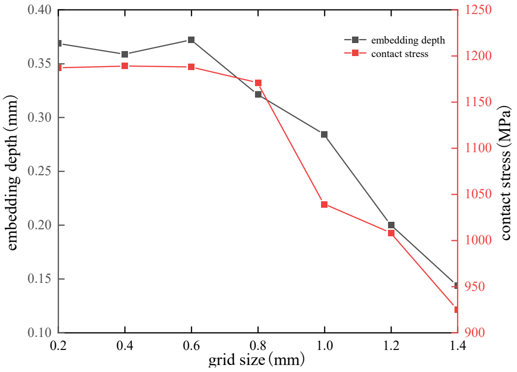

Fig 7. Grid independence verification

Table 1. Mechanical property parameters of materials

Component	Young's modulus E,MPa	Poisson's ratio v	Yield stress σ_s,MPa	Tensile strength σ_b ,MPa
Cone, Slip base	2.26×10^5	0.26	1080	1175
Tooth	6.4×10^5	0.22	5460	—
Casing	1.7×10^5	0.29	965	1210

3.4. Load, Boundary Condition Setting

Based on the downhole operational status of the slip packer, loads and boundary conditions were applied to the model. During cementing, the outer wall of the casing is immobilized by cement, thus a full restraint constraint was imposed on it. The cone, when operational, is constrained from radial motion by the packer body, allowing only axial movement; hence, all degrees of freedom except the axial direction were restricted on the inner wall of the cone, and an axial movement of 38.5mm was used to simulate the axial setting load. During operation, the slips move radially under the compression of the cone to achieve anchoring, thus, degrees of freedom beyond the radial direction were constrained at the lower end face of the slip base. A tie constraint was applied between the slip base and the teeth inserts. Given that all components are made of steel, the friction coefficient at all contact interfaces within the model was set to 0.1.

3.5. Analysis of Simulation Result

To facilitate the observation of stress distributions within the casing, teeth, and slip base along the axial direction, as well as the tooth penetration depth, 2D contour slices were generated along the central axis of the tooth groove. Figures 8, 9, and 10 present simulation contours of the casing inner wall, tooth inserts, and slip base, respectively, during slip anchoring. Figure 8 clearly shows that the equivalent stress values on the casing inner wall decrease sequentially downwards along the axial direction upon contact with the tooth inserts, indicating significant stress inhomogeneity, which may compromise the anchoring effectiveness of the slips to some extent.Figure 9 reveals a gradual decrease in equivalent stress along the axial direction of the tooth inserts, with evident stress distribution inhomogeneity.Figure 10 displays the stress contour of the slip base, where notable stress distribution inhomogeneity among different tooth groove rows is apparent. To enhance the anchoring performance of the tooth-embedded slips, optimization of their structural parameters is necessary.

4. OPTIMAL SELECTION OF SLIP STRUCTURE PARAMETERS

4.1. Effect of Tooth Height h on Anchoring

A nonlinear finite element analysis involving contact mechanics was conducted for the cone-slip-casing system. The other structural parameters remain unchanged, and *h* is set as 5.5mm, 6mm, 6.5mm, and 7mm respectively. The simulation results are shown in the Table 2

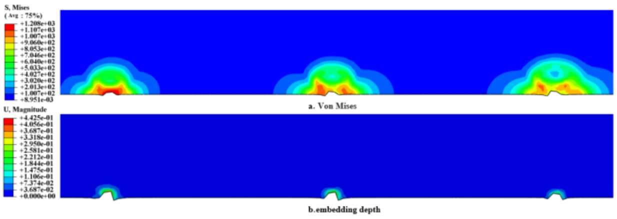

Fig 8. Casing inner wall simulation cloud image

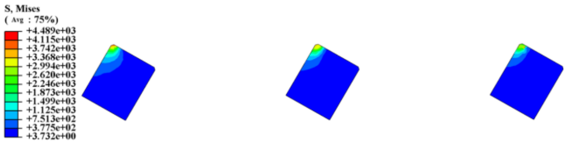

Fig 9. Inserted tooth simulation cloud image

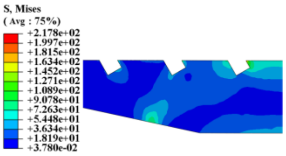

Fig 10. Slip base simulation cloud image

As can be seen from Table 2 , when *h*=6.5mm, the Von Mises stress of casing was minimal, but the plastic deformation of casing was large. When *h*=7mm, the depth of insert slip tooth into casing is the shallowest, but the casing stress is close to the material yield limit. When *h*=6mm, the casing contact pressure is the largest and the matrix stress is the smallest. As can be seen from Fig.11, when *h*=6mm, the stress difference between the front, middle and back rows is the smallest and the stress distribution is more uniform; when *h*=7mm, the stress of the front rows is the smallest and the anchoring effect is the worst; when *h*=5.5mm, the stress difference between the front rows and the middle and back rows is the largest, and the stress distribution is seriously uneven. After comprehensive analysis, *h*=6mm and 6.5mm were taken as the optimum tooth height.

4.2. Effect of Tooth Diameter d on Anchoring

The other structural parameters remain unchanged, and *d* is set as 4mm, 5mm, 6mm, 7mm respectively. The simulation results are shown in the Table 3.

It can be seen from Table 3 that with the increase of insert diameter, the maximum Von Mises stress and contact pressure of casing gradually decreased, and when *d*=4mm, 5mm and 6mm, the maximum stress of casing was close to the yield limit of material. At the same time, it is found that the change of insert diameter has little effect on the plastic strain of casing. As shown in Fig.12, when *d*=7mm, the stress distribution of the front, middle and rear teeth is relatively uniform. After comprehensive analysis, *d*=7mm was taken as the optimum diameter of slip insert teeth.

4.3. Effect of Circumferential Angle θ on Anchoring

The other structural parameters remain unchanged, and *θ* is set as 8°, 10°, 12° respectively. The simulation results are shown in the Table 4.

It can be seen from Table 4 that when *θ*=8°, the maximum Von Mises stress value of casing was the minimum, and when *θ*=12°, the casing stress value was at the strength limit, and it could be seen that circumferential angle had little effect on the equivalent plastic strain of casing. As can be seen from Fig.13,when *θ*=12°, the front tooth stress is the smallest and the anchoring ability is the worst; when *θ*=10°, the front tooth stress is the largest, the stress distribution is the most uniform, and the anchoring ability is the best. Comprehensive analysis, *θ*=8°, 10° as the optimal circumferential angle.

4.4. Effect of Slip Base Wedge Angle γ on Anchoring

The other structural parameters remain unchanged, and *γ* is set as 12°, 15°, 18° respectively. The simulation results are shown in the Table 5.

It can be seen from Table 5 that when the slip base wedge angle *γ*=12° and 15°, the maximum Von Mises stress of casing tends to the casing yield limit, and the plastic strain of casing reaches the maximum when *γ*=12°. As can be seen from Fig.14,when *γ*=12°, the stress value of the front row teeth is the smallest, and the anchoring effect is the worst; when *γ*=18°, the stress difference of the front, middle and back rows of inserts is the smallest, and the stress distribution of different rows of teeth is more uniform. After comprehensive analysis, *γ*=18° is taken as the optimum wedge angle of slip base.

4.5. Effect of Tine Angle α on Anchoring

The other structural parameters remain unchanged, and *α* is set as 55°, 60°, 65°, 70° respectively. The simulation results are shown in the Table 6.

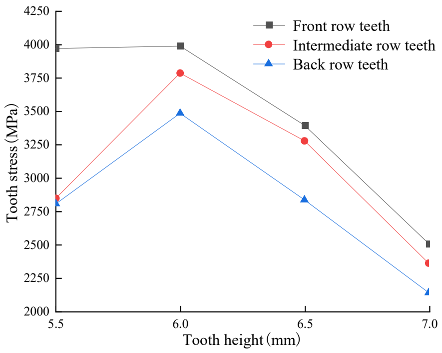

Fig 11. The distribution of tooth stress varies with tooth height

It can be seen from Table 6 that when α=55°, the maximum Von Mises stress of casing was minimal, and when α=60°, the equivalent plastic strain of casing was minimal. As can be seen from Fig.15, when α=60°, the stress of the three rows of teeth reaches the maximum; when α=65° and 70°, the stress difference between the front teeth and the middle and back teeth is large, the stress dispersion is obvious, and the overall anchoring effect of the slips is poor; when α=55°, the stress distribution of the three rows of teeth is more concentrated. After comprehensive analysis, α=55° and 60° were selected as the optimum tine angle.

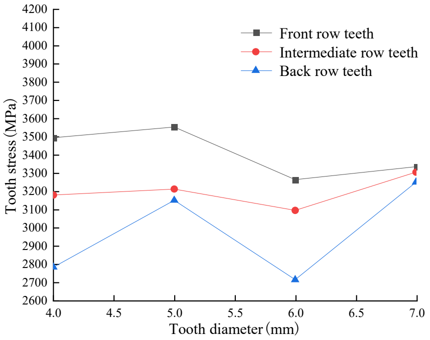

Fig 12. The distribution of tooth stress varies with tooth diameter

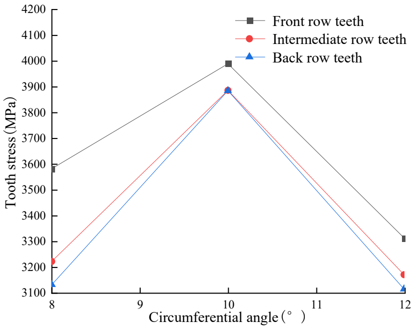

Fig 13. The distribution of tooth stress varies with circumferential angle

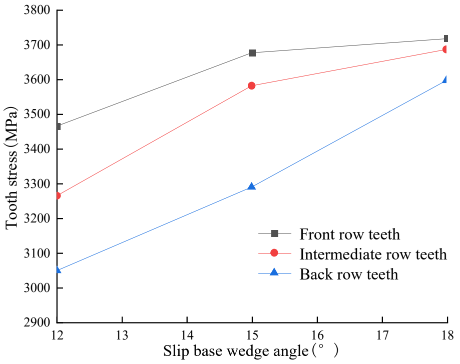

Fig 14. The distribution of tooth stress varies with slip base wedge angle

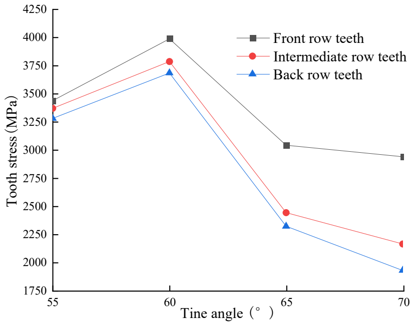

Fig 15. The distribution of tooth stress varies with tine angle

Table 2. Effect of h variation on target parameters

Tooth height h,mm	Casing stress σ_t,MPa	Casing plastic strain ε	Casing contact pressure p,MPa	Slip base stress σ_j, MPa
5.5	1189	0.4728	1241	124.1
6.0	1181	0.3341	2076	107.9
6.5	1165	0.4508	1569	127.0
7.0	1206	0.2916	1560	138.2

Table 3. Effect of d variation on target parameters

Tooth diameter d,mm	Casing stress σ_t,MPa	Casing plastic strain ε	Casing contact pressure p,MPa	Slip base stress σ_j, MPa
4	1210	0.3723	2291	186.3
5	1206	0.3402	1909	115.7
6	1193	0.378	1849	108.6
7	1163	0.3696	1697	115.1

Table 4. Effect of θ variation on target parameters

Circumferential angle θ,°	Casing stress σ_t,MPa	Casing plastic strain ε	Casing contact pressure p,MPa	Slip base stress σ_j, MPa
8	1112	0.3384	1917	114.8
10	1181	0.3341	2076	107.9
12	1206	0.3392	2035	119.0

Table 5. Effect of γ variation on target parameters

Slip base wedge angle γ,°	Casing stress σ_t,MPa	Casing plastic strain ε	Casing contact pressure p, MPa	Slip base stress σ_j, MPa
12	1208	0.4701	2746	217.8
15	1193	0.3341	2068	109.6
18	1105	0.3018	2039	144.2

Table 6. Effect of α variation on target parameters

Tine angle α,°	Casing stress σ_t,MPa	Casing plastic strain ε	Casing contact pressure p,MPa	Slip base stress σ_j, MPa
55	1169	0.4415	1346	144.8
60	1181	0.3341	2076	107.9
65	1177	0.3951	1632	149.1
70	1182	0.3716	1399	141.5

4.6. Parameter Optimization

Table 7. Optimized parameter combination

Combination sequence number	Tooth diameter d,mm	Slip base wedge angle γ,°	Tine angle α,°	Tooth height h,mm	Circumferential angle θ,°
1	7	18	55	6.0	8
2	7	18	55	6.5	10
3	7	18	55	6.0	10
4	7	18	55	6.5	8
5	7	18	60	6.0	8
6	7	18	60	6.5	10
7	7	18	60	6.0	10
8	7	18	60	6.5	8

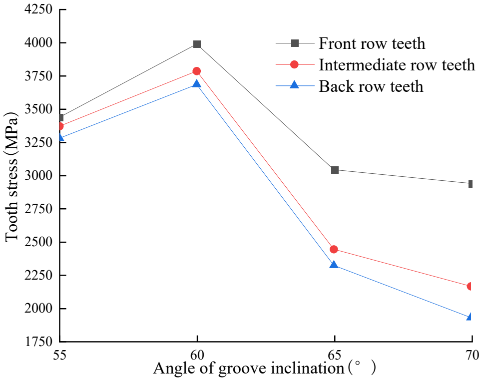

Fig 16. The distribution of tooth stress varies with tine angle

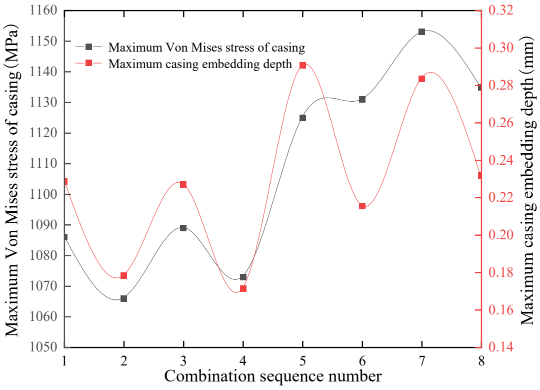

Fig 17. Variation curves of maximum Von Mises stress and maximum embedding depth

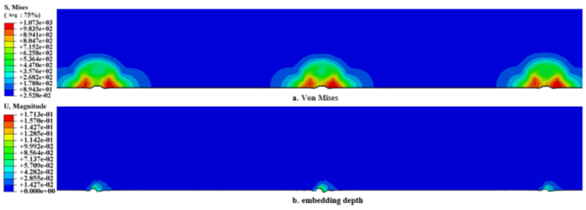

Fig 18. Casing inner wall simulation cloud image

Utilizing orthogonal experimentation, Table7 outlines the optimal combination of the five structural parameters' peak values. The influence curve of each optimization parameter under the combined sequence number from 1 to 8 on the maximum Von Mises stress and maximum casing insertion was shown in Fig.17. Table 8 shows the values of casing embedding depth corresponding to inserts from No. 1 to No. 6 under the optimal combination of slips parameters. Figure 17 underscores that Combinations 2 and 4 feature lower peak Von Mises stresses and casing embedding depths under their respective slip structural configurations. A perusal of Table 8 attests to the fact that the optimized Combination 4 achieves the smallest deviations and variances in the embedment depth of individual teeth, signifying enhanced uniformity in anchoring and effectiveness. Hence, the optimal combination of structural parameters for the inset-tooth slip comprises d=7mm, γ=18°, α=55°, h=6.5mm, and θ=8°. Figures 18, 19, and 20 visually depict the Von Mises stress, indentation depth, and slip base stress distributions, respectively, corresponding to this optimal parameter set, as derived from finite element simulations. A comparative analysis with the contours presented in Section 2.5 reveals that, under identical loading conditions, the optimized casing interior, insert tooth apices, and slip base exhibit substantial stress reductions and more uniform distributions, coupled with decreased casing embedment depths. Additionally, by scrutinizing the optimized outcomes, including equivalent stresses and contact pressures on the insert teeth and casing interior, and juxtaposing them with pre-optimization findings, Figure 21 showcases line graphs contrasting these parameters before and after optimization. The interconnected line segments signify teeth within the same row, whereas distinct lines correspond to distinct rows. Figures 21(a) and 20(b) clearly indicate that, in comparison to pre-optimization, both stress and contact pressure variations among teeth within the same row and across different rows along the slip's axial direction are markedly diminished, attesting to the enhanced uniformity in overall loading post-optimization. Specifically, the maximum insert tooth stress declines by 16.7%, from 4489 MPa to 3741 MPa, while the maximum contact pressure decreases by 13.2%, from 4679 MPa to 4061 MPa.

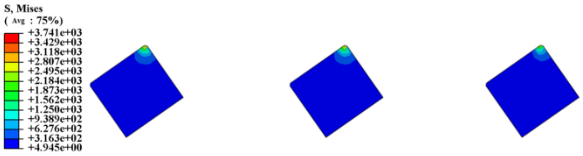

Fig 19. Inserted tooth simulation cloud image

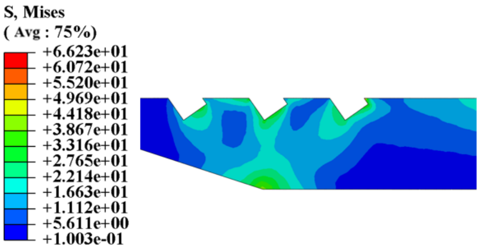

Fig 20. Slip base simulation cloud image

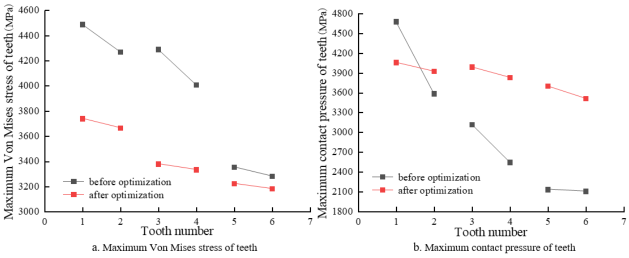

a. Maximum Von Mises stress of teeth
b. Maximum contact pressure of teeth

Fig 21. Corresponding data line chart before and after optimization

Table 8. Tooth embedment depth distribution

Combination	Tooth number						Maximum deviation of embedding depth	Embedding depth variance
	1	2	3	4	5	6		
1	0.2287	0.2266	0.2145	0.2148	0.2123	0.2087	0.0200	6.6×10^{-5}
2	0.1783	0.1723	0.1682	0.1632	0.1622	0.1550	0.0233	6.7×10^{-5}
3	0.2271	0.225	0.2184	0.2167	0.2101	0.2245	0.0170	4.1×10^{-5}
4	0.1713	0.1681	0.1709	0.1698	0.1612	0.1576	0.0137	3.3×10^{-5}
5	0.2907	0.2819	0.2527	0.2592	0.2409	0.2439	0.0498	41.0×10^{-5}
6	0.2155	0.2038	0.2008	0.2008	0.1910	0.1890	0.0265	9.0×10^{-5}
7	0.2695	0.2736	0.2835	0.2835	0.2405	0.2480	0.0430	33.0×10^{-5}
8	0.2214	0.2319	0.1977	0.1967	0.1907	0.1886	0.0433	31.0×10^{-5}

5. CONCLUSION

In this paper, with inserted slips as the research object, finite element analysis and orthogonal test method are used to study the anchoring effect of inserted slips and TP140V steel grade casing. The research conclusions are as follows:

(1)The working force of insert slips is analyzed theoretically, the calculation formula of insert stress when inserted slips are inserted into casing is derived, and the relationship between inserted tooth stress and tooth diameter, Angle of tooth inclination and slip base wedge angle is obtained.

(2)Using maximum Von Mises stress and maximum embedments as evaluation criteria, orthogonal test method was used to select the best structural parameter combination of inserted slips combined with the maximum deviation and variance of embedding depth: tooth diameter d=7mm, slip base wedge angle $\gamma=18°$, tine angle $\alpha=55°$, tooth height h=6.5mm and circumferential angle $\theta=8°$. The maximum Von Mises stress was reduced from 1208MPa to 1073MPa, and the embedding depth was reduced from 0.4425mm to 0.1713mm.

(3)After optimization, the overall force of slips is more uniform. The maximum stress of inserted tooth after optimization is 3741MPa, which is 16.7% lower than before optimization. The maximum contact pressure is 4061MPa, which is 13.2% lower than before optimization.

REFERENCES

[1] Ding, L. L.; Lian, Z. H.;Chen, S. C.;Yang, B. G.;Wei, C. X. 2011. Numerical simulation of wellbore temperature during high-pressure deep well kills, Oil Drilling & Production Technology 33(04): 15-18.http:// dx.doi. org/ 10.13639/j.odpt.2011.04.008.

[2] Wang, Z. M.; Wen, Z. X.;He, Z. J.;Chen, R. Y.;Shi, H. C.;Chen, X. 2022. Characteristics and enlightenment of new progress in global oil and gas exploration in recent ten years, China Petroleum Exploration 27(02): 27-37. http:// dx. doi. org/10.3969/j.issn.1672-7703.2022.02.003.

[3] Su, Y. N.; Lu, B. P.;Liu, Y. S.;Zhou, Y. C.;Liu, X. S.;Liu, W.;Zang, Y. B. 2020. Status and research suggestions on the drilling and completion technologiesfor onshore deep and ultra deep wells in China, Oil Drilling & Production Technology 42(05): 527-542. http://dx.doi.org/10.13639/j.odpt.2020.05.001.

[4] Sun, J. S.; Liu, W.;Wang, Q.;Huang, H. C.;Ji, G. D. 2024. Challenges and Development Prospects of Oil and Gas Drilling and Completion in Myriametric Deep Formation in China, Drilling & Production Technology 47(02):1-9.http:// dx.doi.org/10.3969/J.ISSN.1006-768X.2024.02.01.

[5] Wang, H. G.; Zhang, J. W; Hang, H. C.;Ji, G. D.;Hao, C. 2024. Inspiration and Practice of Drilling and Completion in 10 000-Meter Ultra-Deep Wells in the Gulf of Mexico, Petroleum Drilling Techniques 52(02):12-23.http:// dx.doi.org/10.11911/syztjs.2024121.

[6] She, C. Y. 2024. Progress in ultra-deep drilling and completion technology in the Sichuan Basin and its implications for extra-deep wells of more than ten thousand meters in depth, Natural Gas Industry 44(01):40-48. http://dx. doi. org/10.3787/j.issn.1000-0976.2024.01.004.

[7] Tian, K.; Wang, L.;Hu, L.;Zhang, X; Zhou, X. F. 2018. Development of Non-API Specification TP140V Casing for Service in Extra-deep Complex Well, Steel Pipe 47(01):13-17. http://dx.doi.org/10.3969/j.issn.1001-2311. 2018. 01.002.

[8] Lu, X. Q.; Zhong, S. M.;Li, J. 2011. Design,Development and Application of TP140V Extra-high Strength Oil Casing for Extra-deep Complex Well Service, Steel Pipe 40(05):26-30. http://dx.doi.org/10.3969/j.issn.1001-2311. 2011. 05.006.

[9] Chen, K. P.; Shi, X. X;Mi, Y. F.;Zhang, X. G.;Zhan, F. 2021. Development and Application Status and Development Direction of Non-standard Oil Casing in China, Science & Technology of Baotou Steel 47(03):95-98. http://dx. doi.org/ 10.3969/j.issn.1009-5438.2021.03.027.

[10] Cui, L. B.; Fan, L. Y;Zou, W.;Xie, J.;Zhang, L. Y. 2022. Failure factor analysis and improvement countermeasures of recyclable casing packer in ultra-deep wells in Shunbei Oilfield, Well Testing 31(01):22-26. http://dx. doi.org/ 10.19680/j.cnki.1004-4388.2022.01.004.

[11] Yang, D.; Dou, Y. H.;Xu, A. R. 2008. Causes and countermeasures of acid compression packer loss of high temperature and high pressure deep well, China Petroleum Machinery 36(9):129-131.

[12] Hua, Q.; Qing, Y. B. 2018. Analysis of common causes of seal failure of high-temperature and high-pressure completion packers, Petrochemical Industry Technology 25(10):202. http://dx.doi.org/10.3969/j.issn.1006-0235. 2018. 10.159

[13] Zhao, Y. P.; Li, H. H.;Xie, J.;Fan, L. Y.;Jiao, S. Q.;Hu, Y. 2016. Analysis of Failure Factors of Casing Packer During Completion and Oil Testing and Countermeasures, Technology Supervision in Petroleum Industry 32(04):52-56. http://dx. doi.org/10.3969/j.issn.1004-1346.2016.04.014.

[14] Deng, C. 2022. Research of bionic friction-enhanced surface and micro-tooth marks technologyof packer slip, Xi'an Shiyou University.

[15] Wang, Q.; Kong, C.;Tang, R.;Feng, W.;Li, Y.;Yang, M. 2023. Optimum Design for Inserted Tooth Slips Setting Process Based on the Furrow Effect, Processes 573. https://dx.doi.org/10.3390/pr11020573.

[16] Zhang, D. R.; Chen, Y.;Zhou, W.;Yang, R. W. 2016. Structural Optimization of The Slip of Drillable Bridge Plug, Machinery Design & Manufacture (08):219-223. https://dx.doi.org/10.3969/j.issn.1001-3997.2016.08.060.

[17] Yu, B.; Zhao, W. B.;Lei, L. Q.;Lian, Z. H.;Lin, T. J. 2013. Finite Element Analysis of Inserted Tooth Slips of Non-metallic Bridge Plug and Optimization, China Petroleum Machinery 41(08):68-70+75.https:// dx.doi.org/ 10.3969/ j.issn.1001-4578.2013.08.017.

[18] Wang, Z. J.; Deng, W. D.;Lin, Z. C.;Shang, X. F.;Wang, Y. 2013. Finite element analysis and structure improvements of packer slip in horizontal wells, Oil Drilling & Production Technology 35(04):78-81. https://dx. doi. org/10.3969/j.issn.1000-7393.2013.04.021.

[19] Feng, W. R.; Kong, C. Y.;Zhang, D. R. 2017. Setting process numerical analysis of inserted tooth slip of sidetracking packer based on plough effect, Journal of Machine Design 34(06):55-59. https://dx.doi.org /10. 13841/j. issn. jxsj. 2017.06.011.

[20] Lu, J. K.; Guan, Z. R.;Luo, F. S. 2022. The Analysis of the Soluble Bridge Plug Inserted Slip Base, Mechanical & Electrical Engineering Technology 51(03):122-126. https://dx.doi.org/10.3969/j.issn.1009-9492.2022.03.025.

[21] Cui, L.; Zou, F.; Cheng, J. R.;Wang, P.;Li, Z.;Dou, Y. H. 2023. Sealing Characteristics of All-metal Soluble Bridge Plug Special-Shaped Contact Structure, Lubrication Engineering 48(09):33-40. https://dx.doi.org/ 10.3969/ j.issn. 0254-0150.2023.09.004.

[22] Han, C. J.; Peng, X. F.;Li, L. T. 2020. Anchoring mechanical behavior of packer slips and its HTHP experimental analysis, Natural Gas Industry 40 (07): 76-82. https://dx.doi.org/10.3787/j.issn.1000-0976.2020.07.009.

[23] Pang, L.; Liu, G. C.;Lu, J. P. 2015. The experiments for mechanical properties of 20Cr2Ni4 steel and the coefficient definition of constitutive equation, IOP Conference Series: Materials Science and Engineering 103(1):012028. https: // dx.doi.org/10.1088/1757-899X/103/1/012028.